Surf zone eddies coupled with rip current morphology

Jamie H. MacMahan
Oceanography Department, Naval Postgraduate School, Monterey, California, USA

Ad J. H. M. Reniers
Civil Engineering and Geosciences, Delft University of Technology, Delft, Netherlands

Ed B. Thornton and Tim P. Stanton
Oceanography Department, Naval Postgraduate School, Monterey, California, USA

Received 5 August 2003; revised 2 April 2004; accepted 28 April 2004; published 1 July 2004.

[1] Energetic very low frequency (VLF; frequencies <0.004 Hz) surf zone eddies (SZEs) were observed on a beach composed of shore-connected shoals with quasi-periodic (~125 m) incised rip channels at Sand City, Monterey Bay, California. Incident waves consisted of predominantly shore-normal narrow-banded swell waves. SZEs were located outside the gravity region in alongshore wave number, k_y, spaced within the VLF band, and did not appear to exist in higher-frequency bands. The SZEs were significant ($U_{\mathrm{rms,VLF}} \sim 0.25$ m/s) and constant in intensity within the surf zone (shore-connected shoals and rip channels) and rapidly decreased offshore. The alongshore and cross-shore SZE velocity variances were similar in magnitude. VLF SZE velocities were not forced by VLF surface elevations and were not well correlated with rip current flows ($r^2 = 0.18$). There is an indication that the SZEs were related to wave forcing, with the SZEs statistically correlated with incoming sea-swell wave height ($r^2 = 0.49$). F-k_y spectral estimates illustrate a strong relationship between rip channel spacing and SZE cross-shore velocities ($k_y = \pm 0.008$ m^{-1}) and minimal SZE alongshore velocity variation ($k_y = 0$ m^{-1}). Data analysis suggests that the SZEs are not simply instabilities of an unstable rip current jet. A simple conceptual model suggests that SZE f-k_y spectra can be explained by the entire rip current circulation cells oscillating predominantly in the cross shore and slightly in the alongshore. *INDEX TERMS:* 4546 Oceanography: Physical: Nearshore processes; 3020 Marine Geology and Geophysics: Littoral processes; 4512 Oceanography: Physical: Currents; 4599 Oceanography: Physical: General or miscellaneous; *KEYWORDS:* rip currents, surf zone, nearshore, eddies, circulation, waves

Citation: MacMahan, J. H., A. J. H. M. Reniers, E. B. Thornton, and T. P. Stanton (2004), Surf zone eddies coupled with rip current morphology, *J. Geophys. Res.*, *109*, C07004, doi:10.1029/2003JC002083.

1. Introduction

[2] Velocity measurements within the surf zone for field experiments on planar and barred beaches illustrate that low-frequency (infragravity) motions are ubiquitous. Infragravity (0.004–0.04 Hz) motions are often the dominant energy on the beach compared to the energy within the sea-swell frequency band [*Suhayda*, 1974; *Huntley*, 1976; *Huntley et al.*, 1981; *Holman*, 1981; *Wright et al.*, 1982; *Guza and Thornton*, 1985], even for a beach with persistent rip channels [A. J. H. M. Reniers et al., Modeling infragravity motions on a rip-channel beach, submitted to *Coastal Engineering*, 2004, hereinafter referred to as Reniers et al., submitted manuscript, 2004; J. T. MacMahan et al., RIPEX—Rip currents on a shore-connected shoal beach, submitted to *Marine Geology*, 2004, hereinafter referred to as MacMahan et al., submitted manuscript, 2004]. Infragravity energy is confined to a region within f-k_y space defined by the zero mode edge wave ($f \geq f_o$; $|k_y| \leq k_{yo}$) (Figure 1).

[3] Energetic vorticity motions (nongravity motions), typically occurring at frequencies less than infragravity motions, coexist in the surf zone. The distinction between gravity waves and vorticity motions is determined through frequency-wave number (f-k_y) spectral estimates. We define nongravity motions for frequencies less than 0.004 Hz as very low frequency motions (VLFs) since infragravity waves in the literature have traditionally been referred to as low-frequency motions. Furthermore, VLFs are considered to be predominantly composed of surf zone eddies (SZEs), owing to the relatively small space within the gravity restoring region for frequencies less than 0.004 Hz. (Figure 1).

0148-0227/04/2003JC002083$09.00

Report Documentation Page

Form Approved
OMB No. 0704-0188

1. REPORT DATE	2. REPORT TYPE	3. DATES COVERED
2004		**00-00-2004 to 00-00-2004**

4. TITLE AND SUBTITLE	5a. CONTRACT NUMBER
Surf Zone Eddies Coupled With Rip Current Morphology	5b. GRANT NUMBER
	5c. PROGRAM ELEMENT NUMBER
6. AUTHOR(S)	5d. PROJECT NUMBER
	5e. TASK NUMBER
	5f. WORK UNIT NUMBER
7. PERFORMING ORGANIZATION NAME(S) AND ADDRESS(ES) **Oceanography Department,Naval Postgraduate School,Monterey,CA**	8. PERFORMING ORGANIZATION REPORT NUMBER
9. SPONSORING/MONITORING AGENCY NAME(S) AND ADDRESS(ES)	10. SPONSOR/MONITOR'S ACRONYM(S)
	11. SPONSOR/MONITOR'S REPORT NUMBER(S)

12. DISTRIBUTION/AVAILABILITY STATEMENT
Approved for public release; distribution unlimited

13. SUPPLEMENTARY NOTES

14. ABSTRACT

15. SUBJECT TERMS

16. SECURITY CLASSIFICATION OF:			17. LIMITATION OF ABSTRACT	18. NUMBER OF PAGES	19a. NAME OF RESPONSIBLE PERSON
a. REPORT **unclassified**	b. ABSTRACT **unclassified**	c. THIS PAGE **unclassified**	**Same as Report (SAR)**	**15**	

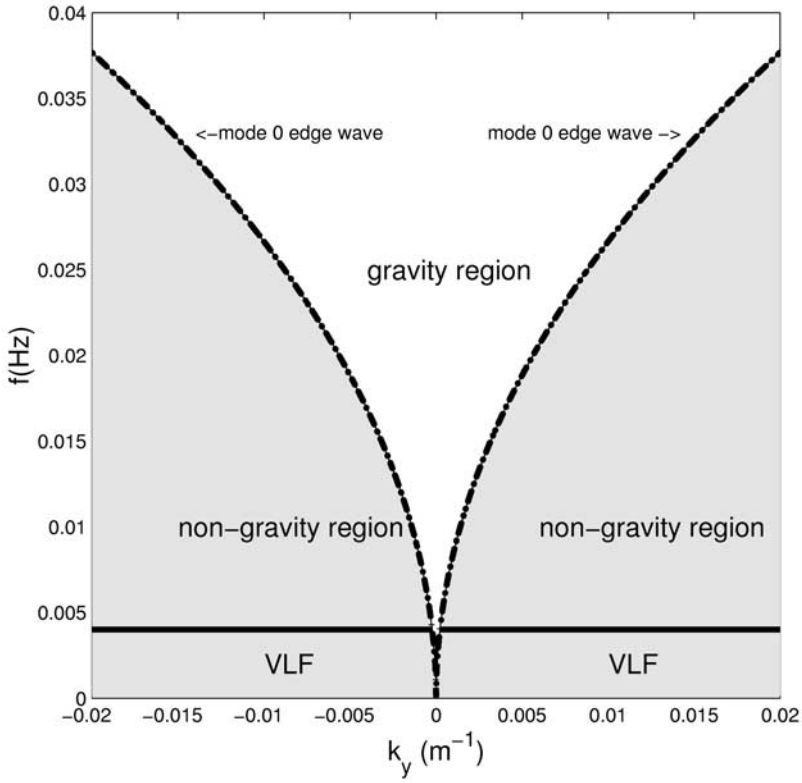

Figure 1. F-k_y spectrum illustrating gravity and nongravity region separated by mode 0 edge wave. The very low frequency (VLF) motions are further defined in the nongravity region for frequencies less than 0.004 Hz.

[4] Most nearshore studies have associated SZEs with shear instabilities of the longshore current. In 1989, *Oltman-Shay et al.* [1989] discovered energetic motions in the longshore current located within the nongravity regions in f-k_y space (Figure 1), ranging in frequencies from 0 to 0.045 Hz. These motions were most energetic for frequencies less than 0.004 Hz (i.e., VLFs), decreasing in energy with higher frequencies. The longshore current instabilities have a near-linear dispersion relationship in f-k_y space related to the shear, speed, and direction of the longshore current [*Bowen and Holman*, 1989; *Oltman-Shay et al.*, 1989; *Noyes et al.*, 2004].

[5] Field investigations of topographically controlled rip currents [*Shepard and Inman*, 1950; *Sonu*, 1972; *Aagaard et al.*, 1997; *Smith and Largier*, 1995; *Brander*, 1999; *Brander and Short*, 2000, 2001; *MacMahan et al.*, 2004] documented rip current velocity pulsations within the infragravity frequency band. In addition to the energetic rip current pulsations, energetic VLF motions have also been observed within rip current systems. *Smith and Largier* [1995] acoustically measured rip current motions outside the breaker zone and found that they fluctuated aperiodically with temporal scales greater than 15 min. *Haller and Dalrymple* [2001] documented oscillations of the rip current jet-like motions in a laboratory study, referred to as rip current instabilities.

[6] Most previous field experiments have either overlooked the amount of energy associated with VLFs by not sampling sufficiently long to resolve them or attributed these signals to infragravity motions. *Brander and Short* [2001] reexamined their original observations by *Brander* [1999] and found VLFs in their measurements. *Ogston and Sternberg* [2003] re-analyzed measurements obtained by *Beach and Sternberg* [1988] in the surf zone, using longer records, and found that there was a significant amount of energy in the VLF band for both velocity and sediment concentration measurements. Thus VLFs also may be ubiquitous within the surf zone and are believed to be related to forced surf zone eddies.

2. Field Site

[7] Observations were obtained on a beach with quasi-periodically spaced rip current channels at Sand City, Southern Monterey Bay, California, during the Rip Current Field Experiment (RIPEX)-Steep Beach Experiment (SBE) during the months of April and May 2001. The beach face was relatively steep with a slope of about 1:10 with beach cusps O(35 m), which flattens out to a low-tide terrace (1:100) with quasiperiodic O (125 m) incised rip channels, continuing farther offshore with a 1:20 slope (Figure 2). Two primary arrays were deployed: (1) an alongshore array of 6 bidirectional electromagnetic (EM) current meters that traversed the shore-connected shoals and rip channels, and (2) a cross-shore array of pressure and EM current meters on the shore-connected shoal; these sensors were sampled continuously and synchronously at 8 Hz. EM current meters located on the shore-connected shoal were not always submerged at lower tides. An upward looking acoustic Doppler current meter (ADCP) was deployed offshore of the rip channel and sampled at 0.1 Hz.

[8] A directional wave rider buoy located ~650 m offshore in 17 m depth measured offshore wave conditions. Considerable variation in wave characteristics occurred

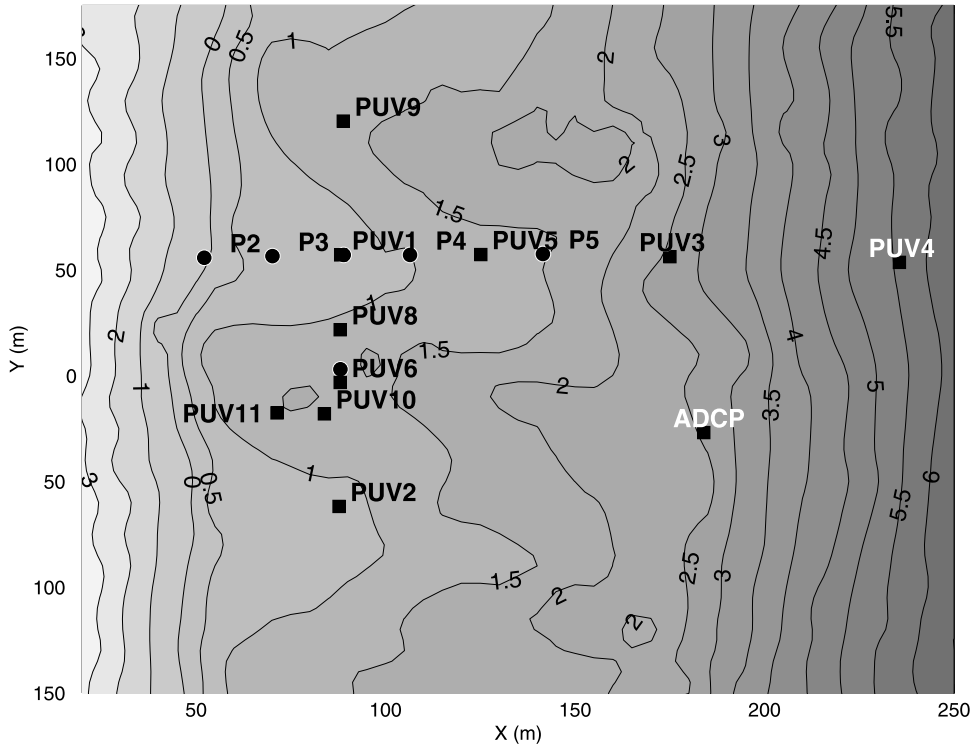

Figure 2. Bathymetry for year day 117 obtained by combining hydrographic survey system mounted aboard a personal watercraft (high tide) and a backpack mounted to a person walking the shoals (low tide). The dots indicate pressure sensors, and squares represent colocated pressure and velocity.

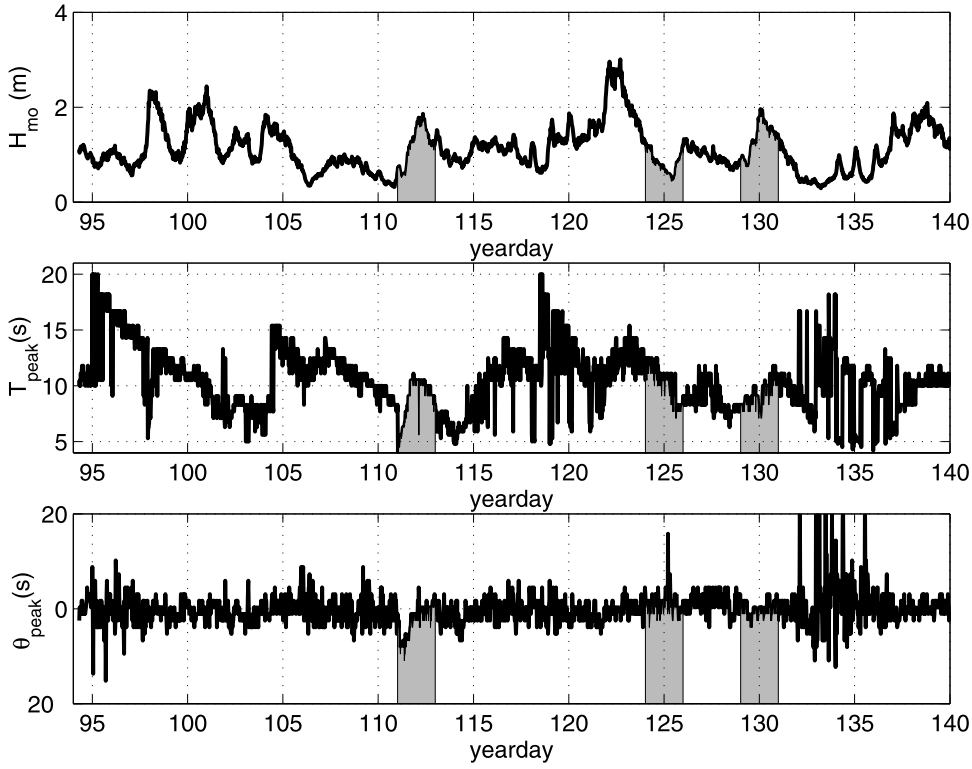

Figure 3. Wave climate measured by directional wave buoy located in 17 m water depth, approximately 650 m offshore, (top) H_{mo}, (middle) peak wave period, and (bottom) peak wave direction. Shaded regions represents periods of measurement discussion.

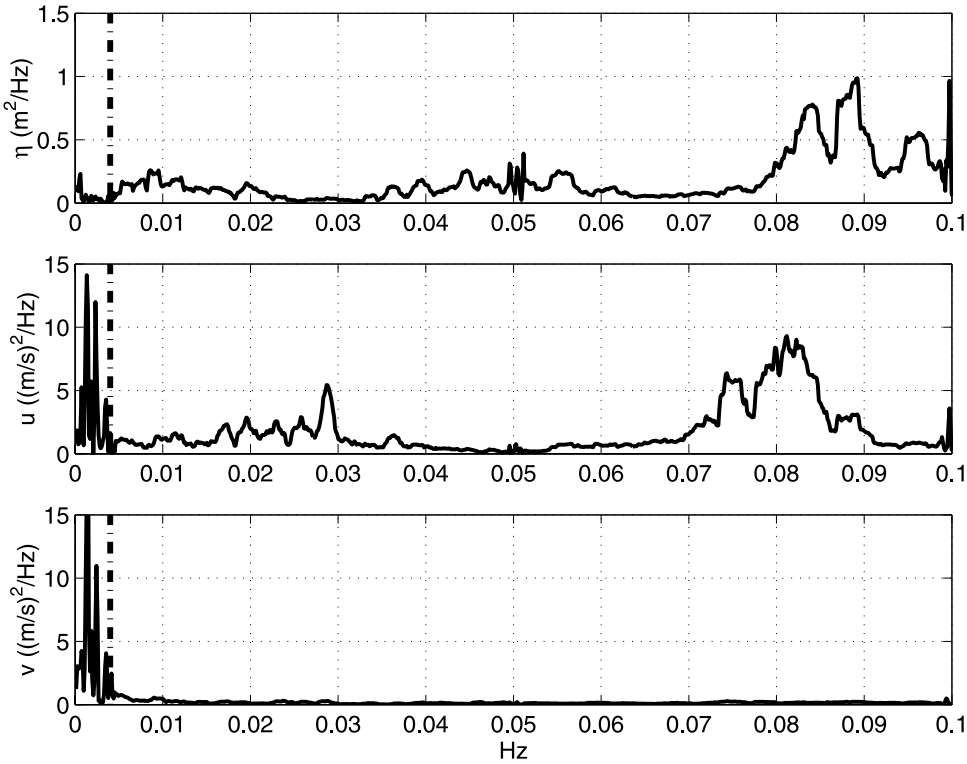

Figure 4. Spectra of (top) pressure, (middle) cross-shore, and (bottom) alongshore velocity for PUV11 located within the rip channel for year day 124.1818. The regions between df −0.004 Hz have a DOF with df of 0.0001 Hz, between 0.004 and 0.05 Hz have 22 DOF with a df of 0.001 Hz and between 0.05 and 0.1 Hz have 42 DOF with a df of 0.0021 Hz. The region to the left of the vertical line at 0.004 Hz represents VLFs.

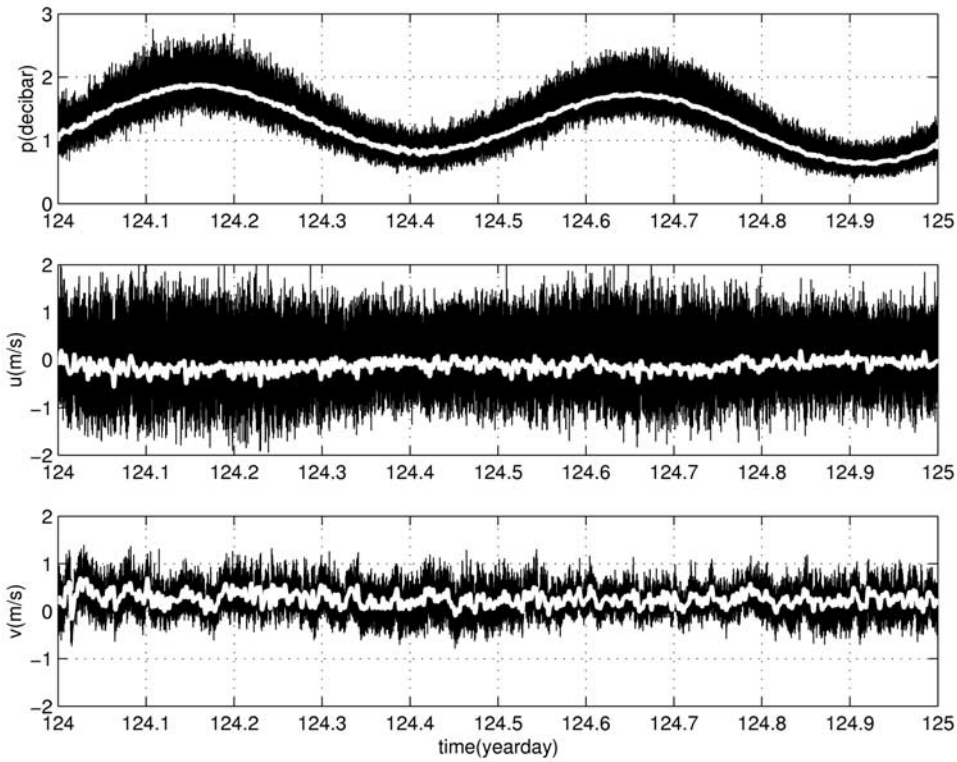

Figure 5. Time series of (top) pressure, (middle) cross-shore velocity, and (bottom) alongshore velocity for PUV11 for year day 124. The black line is the raw signal and the white line in the low-pass filtered signal (FC = 0.004 Hz) representing the VLFs.

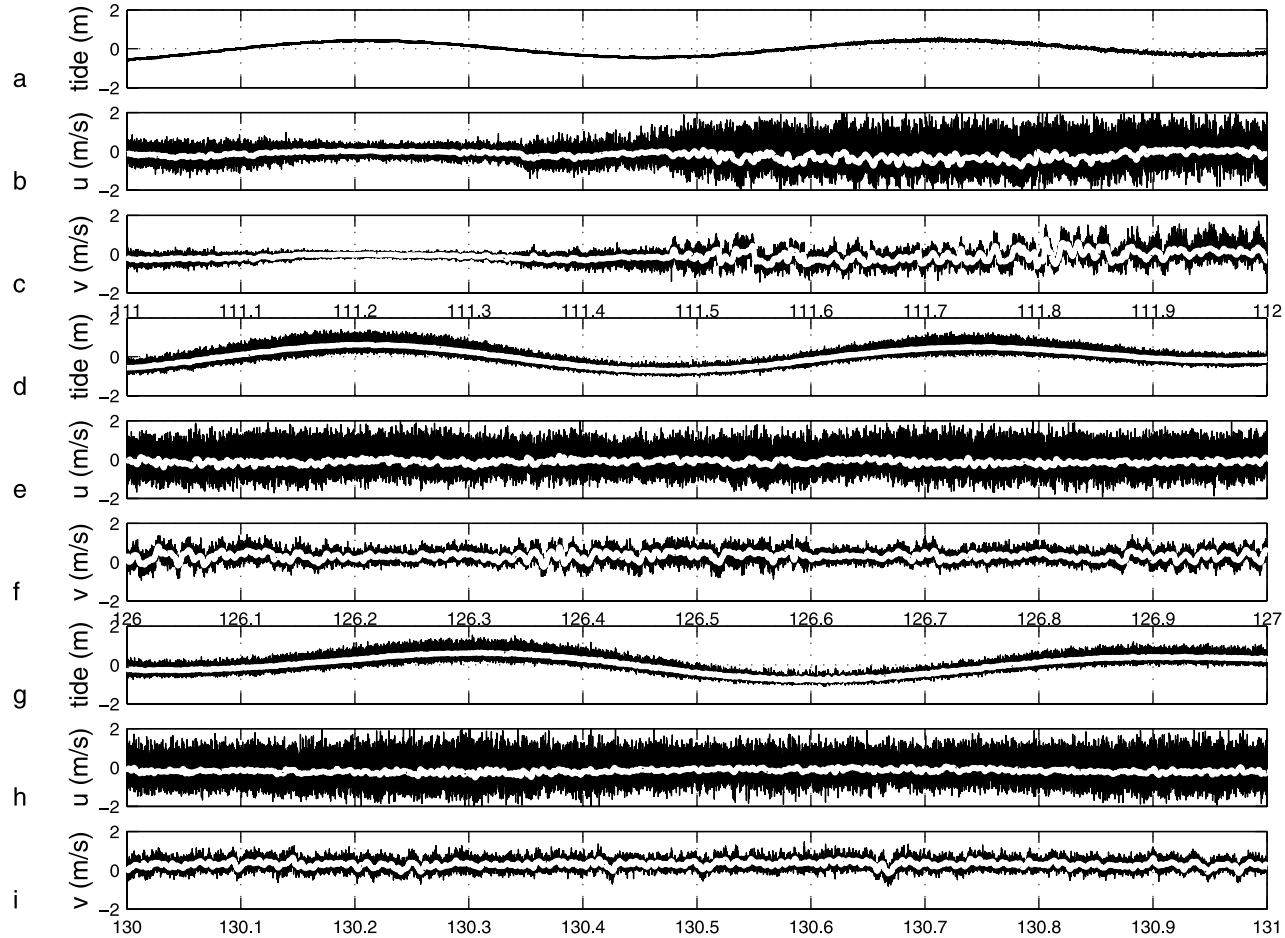

Figure 6. Time series at PUV11 for (a, b, and c) year day 111, (d, e, and f) year day 126, and (g, h, and i) year day 130. The black line is the raw signal for pressure (Figures 6a, 6d, and 6g), cross-shore velocity (Figures 6b, 6e, and 6h), and alongshore velocity (Figures 6c, 6f, and 6i) and the white is the low-pass signal (FC = 0.004 Hz) for each measurement. Note the pressure sensor did not work properly for PUV11 on year day 111.

throughout the experiment (year days 100–140) (Figure 3). In spite of the large temporal variability in wave height and period, the mean wave incidence angle was predominantly shore-normal. Beach face and bathymetry surveys were obtained using a differential kinematic global positioning system (KGPS) mounted on a sonar equipped personal watercraft [*MacMahan*, 2001], in a backpack placed on a person, and on an all-terrain vehicle.

[9] The mean flow field was represented by cellular circulation, with predominant shoreward flow on the shore-connected shoals and seaward flow through the rip channels that persisted throughout the experiment, except for low wave conditions. For an additional discussion of the experiment, see MacMahan et al. (submitted manuscript, 2004).

3. Very Low Frequency Motions

3.1. Observations

[10] Similar to the experience encountered by *Oltman-Shay et al.* [1989], we often experienced significant pulsations during the maintenance and inspection of the EM current meters. Initially, these motions were attributed to infragravity rip current pulsations [*MacMahan et al.*, 2004]. It was not until examining the time series of the current meter data that energetic very low frequency motions (VLFs) were identified, fluctuating on the order of 15 min. Owing to the nearly shore normal waves, there were minimal (if any) longshore currents. Therefore these motions are not associated with the shear instabilities of longshore currents.

[11] To obtain high resolution, spectra was calculated from 2.28-hour records, resulting in frequency resolution (df) of 0.0001 Hz with 2 degrees of freedom (DOF). The total record was quadratically detrended to remove the tidal signature. A significant amount of energy is found within the VLF band for both the cross-shore and alongshore velocity components, while the energy within the sea surface elevations is minimal (Figure 4). Note that energy is significant within the infragravity (0.004–0.04 Hz) and swell and sea (0.04–0.35 Hz) frequency bands for sea-surface elevation and cross-shore velocities and minimal for alongshore velocities.

[12] Examples of VLFs are examined in the low-passed (frequency cutoff (FC) FC = 0.004 Hz) time series for pressure, cross-shore, and alongshore velocity measure-

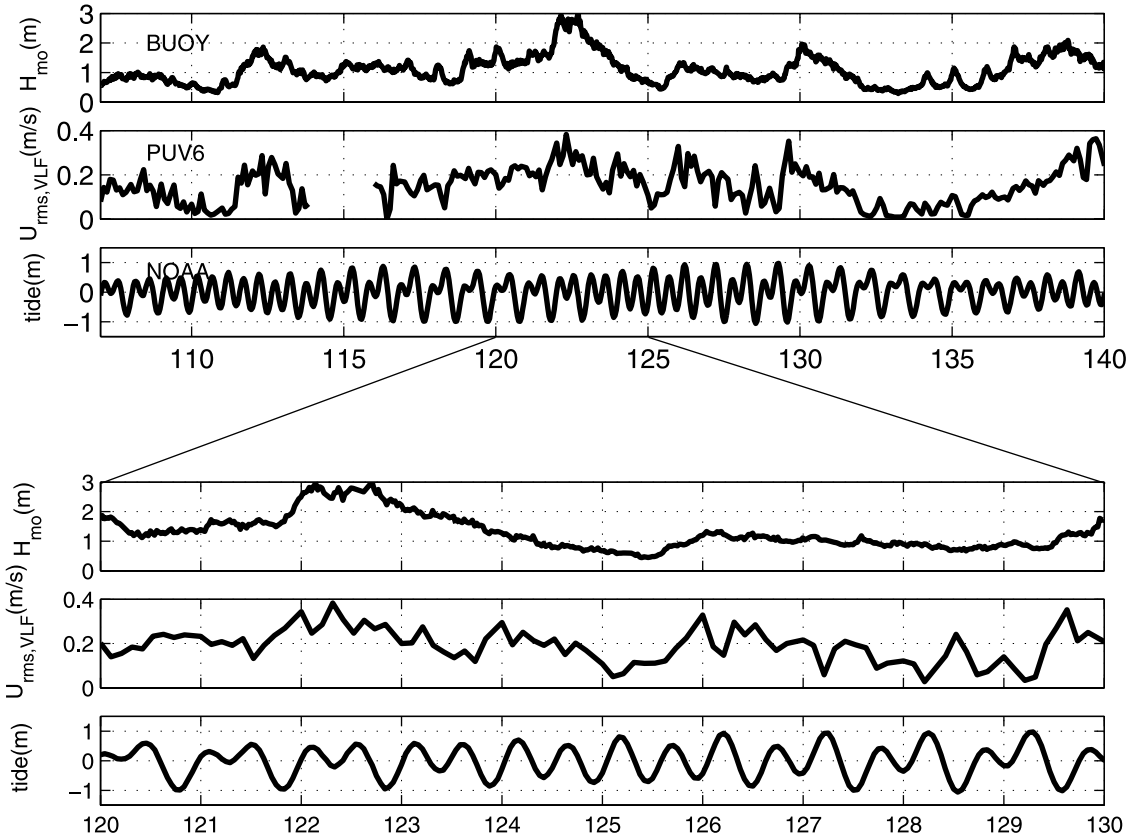

Figure 7. Significant wave height measured at the wave buoy for reference is shown in the first panel. Variance of $U_{\mathrm{VLF,rms}}$ for PUV6 located within the rip channel is shown in the second panel. Tidal elevation measured at the NOAA station for reference is shown in the third panel. The top three plots span the time period for year days 107–140, while the bottom three plots are expanded views of year days 120–130 to examine the tidal variability.

ments on year day 124 for PUV11 located within the rip channel (Figure 5). The pressure signal has minimal VLF signal, whereas the cross-shore and alongshore velocities have significant VLF signals (Figure 5), which are persistent throughout the records.

[13] Different VLF behaviors were observed during the experiment. Time series of sea surface elevations, cross-shore, and alongshore measurements for sensor PUV11 for three days (year days 111, 126, and 130) are examined in Figure 6. For year day 111 the measurements illustrate a segment when there is a dramatic increase in swell energy and the VLFs spin up (Figures 6a, 6b, and 6c). For year day 126 the alongshore component of the VLFs are modulated by the tide with increased VLF velocities occurring at lower tides (Figures 6d, 6e, and 6f), while year day 130 demonstrates a period when the VLFs remain relatively constant throughout the day (Figures 6g, 6h, and 6i). For all three days the alongshore VLF component qualitatively appears larger than the associated cross-shore component.

3.2. VLF Statistics

[14] Low-passed root-mean squared (rms) VLF values for sea surface elevation, cross-shore, and alongshore velocity ($\eta_{\mathrm{rms,VLF}}$, $u_{\mathrm{rms,VLF}}$, $v_{\mathrm{rms,VLF}}$) are obtained by integrating the energy density spectra, E(f), within the 0–0.004 Hz frequency band. Average VLF wave period (first moment wave period, $T_{m01,\mathrm{VLF}}$) was computed instead of peak frequency owing to the sensitivity of the measure to the frequency resolution. The average VLF period is ~13 min for both cross-shore and alongshore VLF motions. The distribution of VLF periods vary slightly between locations. Most VLF periods fall within the 500–1500 s temporal range with mean period of 800 ± 300 s.

[15] The temporal and spatial velocity variations are examined. $U_{\mathrm{rms,VLF}}$, is computed from $\sqrt{u^2_{\mathrm{rms,VLF}} + v^2_{\mathrm{rms,VLF}}}$ to eliminate any potential bias associated with current meter orientation. $U_{\mathrm{rms,VLF}}$ for PUV6 has daily variability, but the overall velocity trend increases with increasing sea-swell energy (Figure 7). Qualitatively, some of the daily variability can be associated with tidal modulation, which results in an inverse relationship with VLF velocities increasing during decreasing tidal elevations. This relationship is visibly evident for year days 126–130 (Figure 7, bottom panel), which is a period of relatively constant sea-swell wave energy. VLF rms values were computed with 75% overlap to provide for continuous measure and band-pass filtered to retain the tidal signature, resulting in an overall VLF tidal significant (95%) correlation of $r = 0.28$.

[16] Total VLF velocity magnitudes ($U_{\mathrm{rms,VLF}}$) were computed for year days 111–120 to examine spatial vari-

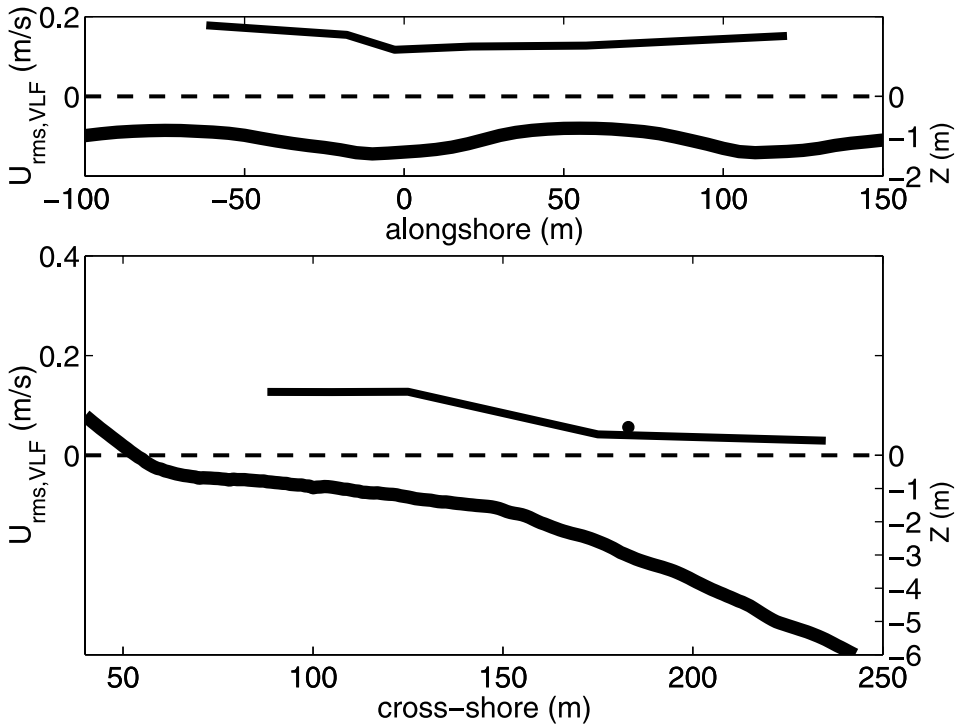

Figure 8. $U_{\mathrm{rms,VLF}}$ averaged over year days 111–120 (top) within the alongshore array and (bottom) in the cross shore. The 95% confidence interval is represented by the thickness of the $U_{\mathrm{rms,VLF}}$ curve. The depth profiles are shown as a thick curve (depth labeled on the right-hand side). $U_{\mathrm{rms,VLF}}$ measured at by the ADCP in the neighboring rip channel is represented by black circle. The dashed line represents zero intensity and mean sea level.

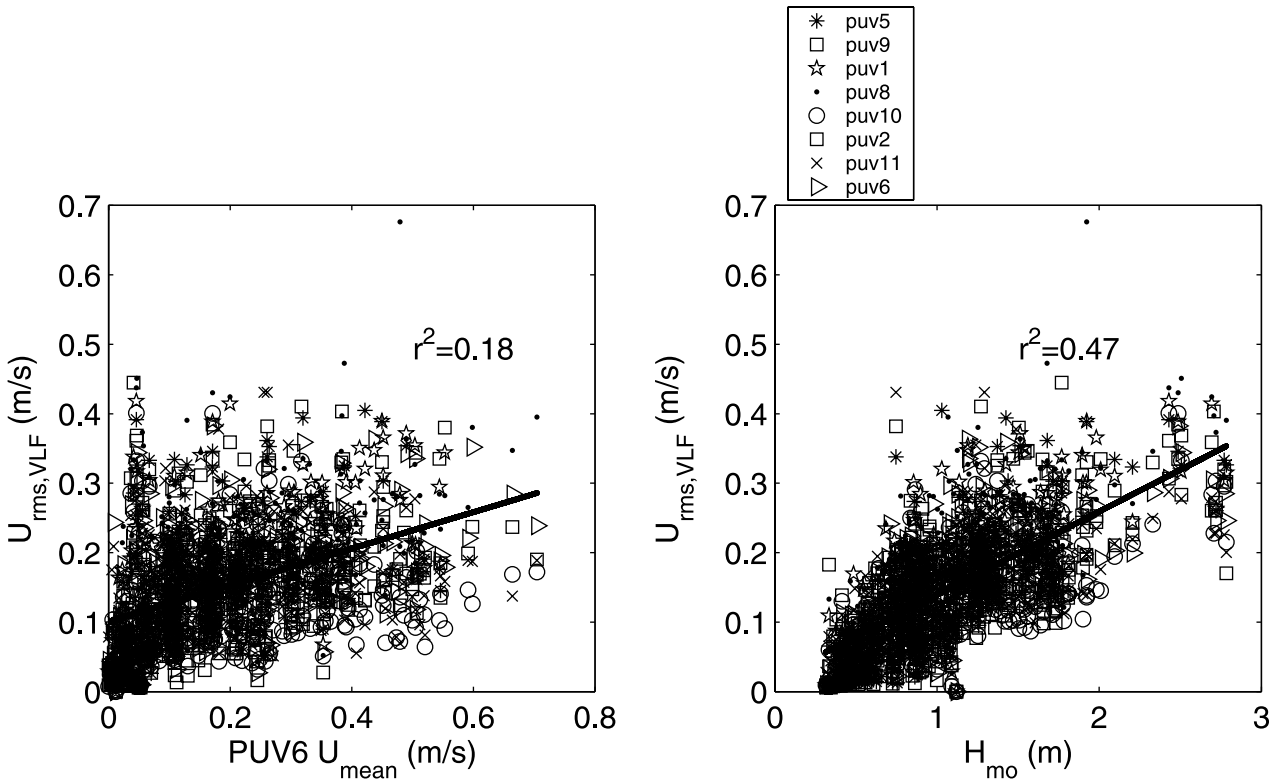

Figure 9. $U_{\mathrm{rms,VLF}}$ plotted versus (left) U_{mean} measured at PUV6 and (right) H_{mo}.

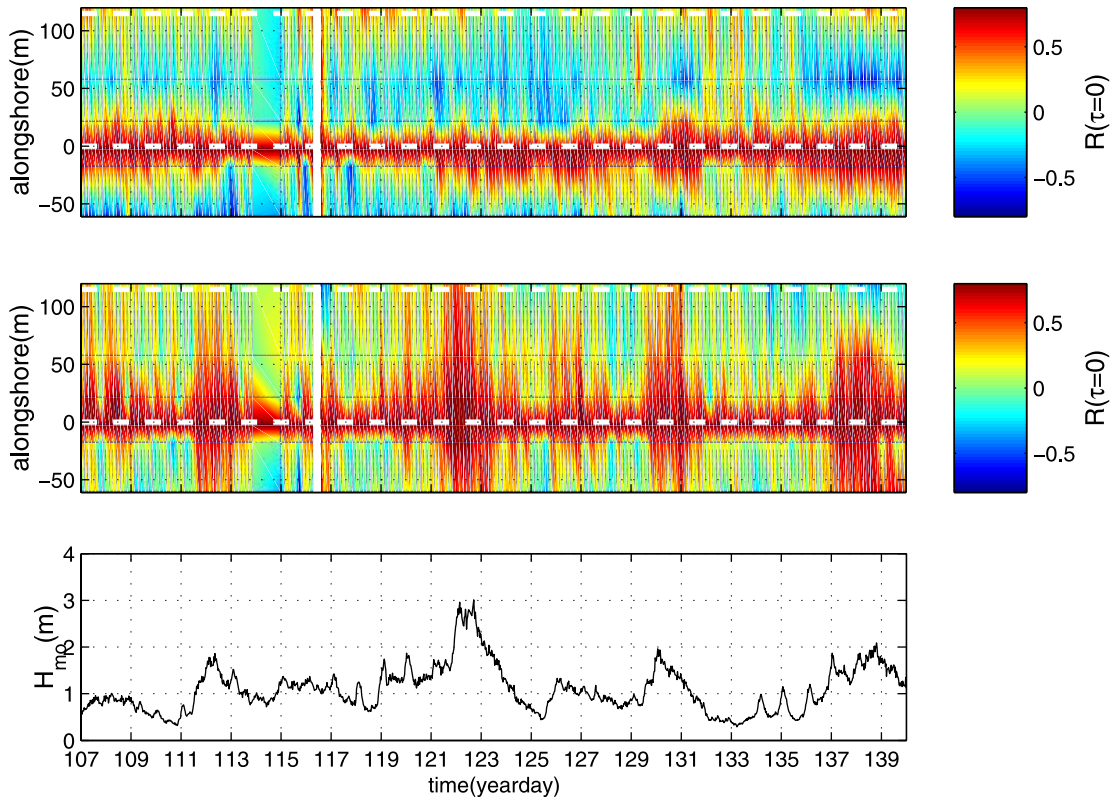

Figure 10. Cross correlations of (top) u_{VLF} and (middle) v_{VLF} with respect to measurements at PUV6 located within the rip channel at $y = 0$ in the alongshore array at zero time lag. Dashed line represents location of the rip channels. (bottom) H_{mo} given for reference.

ability, which is representative of other days throughout the experiment. There are minimal differences in the alongshore transect of $U_{rms,VLF}$ (Figure 8). The 95% confidence interval is the thickness of the line. $U_{rms,VLF}$ is unaffected by the alongshore bathymetric variability of the shore-connected shoals and rip channels (Figure 8) and is not focused within the rip channels, differing from observations by *Haller and Dalrymple* [2001]. This suggests that the observed VLF motions are not a result of rip current instabilities but are developed by a different mechanism. The cross-shore magnitudes are relatively constant within the surf zone but rapidly decay outside the surf zone (Figure 8). Similar VLF values are observed for measurements outside the surf zone of the shore-connected shoal and the rip channel (Figure 8). Thus the VLFs are energetic (~0.2 m/s) within the surf zone with minimal alongshore variability and decrease (~0.05 m/s) outside the surf zone.

[17] An increase in rip velocity should result in an increase in shear as the rip channel width is constrained. If the VLF motions are related to the instabilities of the rip currents, then an increase in rip current velocity shear should increase instability intensities. It has been found that rip current velocities increase with increasing wave energy and decreasing tidal elevation [*Brander and Short*, 2001; *Dronen et al.*, 2002; *Haller et al.*, 2002; MacMahan et al., submitted manuscript, 2004] and that the $U_{rms,VLF}$ qualitatively is related with sea-swell energy and tidal elevation (Figure 7). The $U_{rms,VLF}$ for sensors within the surf zone are plotted correlated with the mean (90 min) rip current velocity for PUV6, which are significantly correlated (r^2 = 0.18) at the 95% confidence level (Figure 9). $U_{rms,VLF}$ has a greater statistically significant (95%) correlation with H_o (r^2 = 0.49) than with U_{mean} (r^2 = 0.18), suggesting that VLFs are influenced by external wave forcing.

3.3. VLF Spatial Behavior

[18] Cross-correlation analysis was performed to determine alongshore spatial relationships of VLFs. The low-passed (<0.004 Hz) cross-shore and alongshore velocities within the rip channel (PUV6) are correlated with adjacent sensors in the alongshore array (PUV1, PUV2, PUV8, PUV9, PUV11) and presented at zero time lag as time stacks (Figure 10). For the VLF cross-shore velocities in the alongshore array, the correlation varies spatially with positive correlation occurring in the rip channels and negative correlation occurring on the shore-connected shoals. The spatially varying correlations suggest a relationship associated with the underlying bathymetry and rip current flow characteristics of vorticity motion. Similar analysis was performed on the VLF alongshore velocities (Figure 10, middle panel). High positive correlation occurs across the alongshore array for the alongshore velocities during energetic wave events. During mild wave conditions the correlation is poor. There was ~800 s time lag associated with the correlation maxima of the cross-shore and alongshore VLF velocities, representative of the $T_{m01,VLF}$ of the measurements.

[19] Frequency wave number (f-k_y) spectra were calculated using the iterative maximum likelihood estimator (IMLE)

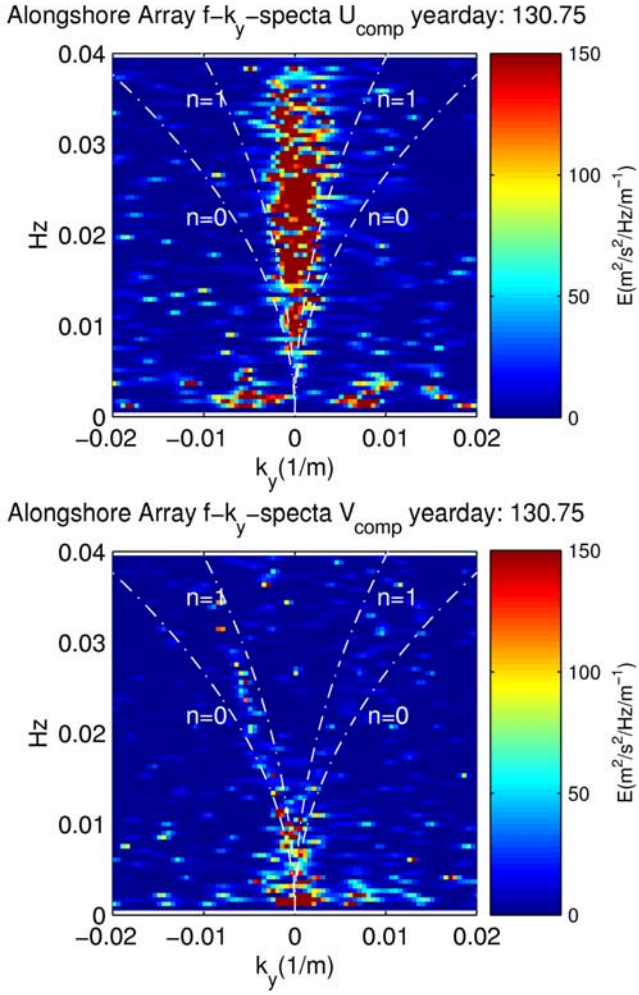

Figure 11. F-k_y spectra computed using IMLE method for (top) cross-shore and (bottom) alongshore velocities for the alongshore array for year day 130.75. The dashed lines represent mode 0 and 1 edge wave dispersion curves based on numerical experiments.

[*Pakwa*, 1983] evaluated by *Oltman-Shay and Guza* [1987] for detection of edge waves and later by *Oltman-Shay et al.* [1989] for the detection of longshore current shear instabilities. A basic assumption of the IMLE is spatial homogeneity, which is not necessarily expected over bathymetry with quasiperiodic rip channels. The IMLE was tested and the comparisons of IMLE field measurements and IMLE and Fourier model simulations suggest the IMLE is applicable for this particular beach (Reniers et al., submitted manuscript, 2004) through comparisons of IMLE field measurements and IMLE and Fourier model simulations. Edge wave dispersion curves for this beach have been determined by numerical experiments, see Reniers et al. (submitted manuscript, 2004).

[20] The energy within the f-k_y spectra is focused within the VLF band (<0.004 Hz) and nongravity region (Figure 1) for both the alongshore and cross-shore velocity (Figure 11). This is unlike the characteristics of shear instabilities of longshore currents, where energy is present at higher frequencies [*Oltman-Shay et al.*, 1989]. For the cross-shore f-k_y spectra (Figure 12, middle panel) the energy within the VLF band is generally concentrated around $k_y = \pm 0.008$ m^{-1} (λ_y = 125 m), approximately equal to rip channel spacing, while for the alongshore f-k_y spectra (Figure 12, bottom panel), energy is generally focused around $k_y = 0$ m^{-1}. It is surprising that there are two different spatial scales associated with the VLFs, whereas longshore current instabilities generally have similar spatial scales for both cross-shore and alongshore f-k_y spectra [*Oltman-Shay et al.*, 1989].

[21] F-k_y spectra were integrated over the VLF bands for year days 107–138, and plotted as a wave number spectra time stack (Figure 12). The energy within the VLF cross-shore velocities is generally focused around rip channel spacings, $k_y = \pm 0.008$ m^{-1}, and higher harmonics of the rip channel spacing throughout the entire experiment. While the energy within VLF alongshore velocity is focused about $k_y = 0$ m^{-1}, suggesting a wavelength that is infinitely long or no alongshore propagation (see below). The energy increases with increasing sea-swell energy.

4. Discussion

4.1. Surf Zone Eddies (SZEs)

[22] *Peregrine* [1998] conceptualized the behavior of free eddies within the surf zone. He hypothesized for a planar beach that a single eddy would travel parallel to the shoreline, while two opposite-signed eddies (dipoles) would induce predominantly cross-shore motion. He also suggested that the eddy migration is limited by deeper water to approximately two surf zone widths. When more than two eddies exist in the surf zone, it is hypothesized that eddies will propagate randomly in the cross shore at various alongshore locations.

[23] *Ryrie* [1983] showed that a single wave group packet approaching the shoreline at an oblique angle with a particular alongshore length produces surf zone eddies (on the order of surf zone scale), which are slowly dissipated by bottom friction. A wave group packet has a particular cross-shore and alongshore spatial scale. *Buhler and Jacobson* [2001] investigated a pair of oblique wave group packets (dipole, two circulation cells of opposite signs), which produced eddies.

[24] Initial observations of SZEs were documented during the nearshore sediment transport study by *Tang and Dalrymple* [1989], who related observations of migrating rip currents on a near planar beach with wave group forcing. This observation was later conceptualized and verified in the laboratory by *Fowler and Dalrymple* [1990]. They documented rip currents (SZEs) propagating slowly at speed, $C \simeq \Delta k/\Delta f$, forced by wave groups formed by two different wave trains from different directions, ($\Delta k_y = k_1 \sin(\theta_1) - k_2 \sin(\theta_2)$ and $\Delta f = f_1 - f_2$). When Δk_y is approximately zero, there is no alongshore propagation (Figures 11 and 12). This mechanism is a generalized version of *Dalrymple*'s [1975] generation of stationary rip currents formed by two intersecting (monochromatic) wave trains at equal and opposing angles. As *Fowler* [1991] increased the number of energetic directional components, the hydrodynamic response in the f-k_y spectra became broader.

[25] *Reniers et al.* [2004] generalized these previous approaches (above) with realistic directional wave spectra and found random patches of wave group packets entering the surf zone. These wave group packets create gradients in

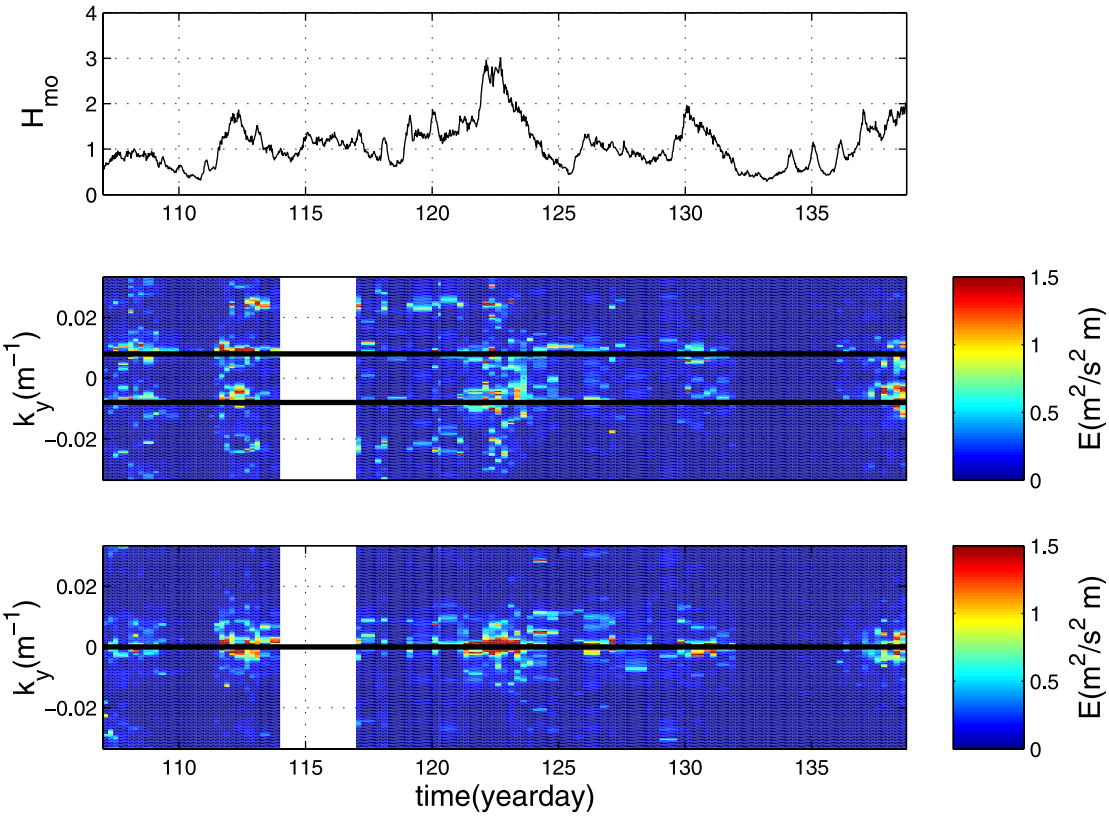

Figure 12. Significant wave height measured at (top) PUV4 provided for reference. Integrated energy within the VLF band for (middle) cross-shore and (bottom) alongshore velocities in the alongshore array. Bold lines represent, for the U_{VLF} k_y time stack, the approximate rip channel spacing ($k_y = \pm 0.008$ m^{-1}), while for the V_{VLF} k_y time stack, $k_y = 0$ m^{-1}.

radiation stresses as the waves break, which force surf zone eddies that have preferential scale based on Δk_y. They found a morphodynamic response of incised rip channels at similar scales.

[26] It is hypothesized that the breaking waves of group packets induced random alongshore gradients in radiation stresses, forcing SZEs with rip currents to oscillate within the RIPEX field measurements. However, as opposed to the SZEs migrating alongshore within the surf zone [*Fowler and Dalrymple*, 1990] or migrating freely [*Peregrine*, 1998], there is morphologic feedback occurring that couples the rip current cells to the underlying bathymetry. The random wave group packets force the cells to oscillate within the surf zone on O(15 min) timescales. This explains the correlation with $U_{\mathrm{rms,VLF}}$ and H_o as well as the large amount of scatter (Figure 10). The complexity of this beach makes it difficult to completely evaluate this process. The SZE rms magnitudes are spatially homogenous within the surf zone (Figure 8). Cross-correlation analysis with the cross-shore velocities suggest eddy behavior with the flows being out of phase between the rip channels and shore-connected shoals (Figure 10). This is further supported by the f-k_y spectral estimates, which suggest eddies that have a morphologic coupling (Figures 11–12).

[27] The spatial scales of the observed f-k_y spectra can be explained by the simple schematic in Figure 13. If rip current cells exist and oscillate within the VLF band in the cross shore, this will produce the spatial scales observed in the f-k_y spectra (Figures 11–12). A predominantly cross-shore displacement (oscillation) will produce energy focused around the rip current spacings for cross-shore velocities. Taking a slice in the alongshore, cross-shore velocities produce a

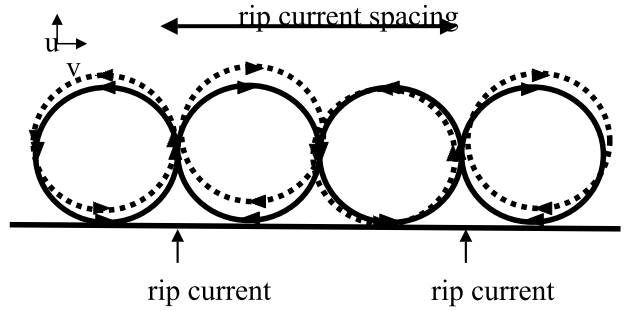

Figure 13. Hypothetical rip current cells at $t = 0$ represented by solid lines. At some time later ($t > 0$), rip current cell are displaced (dashed line). This motion induces alongshore spreading around $k_y = 0$ m^{-1} for the alongshore velocities in the f-k_y spectra, while producing energy at the rip channel spacing for $k_y = \pm 0.008$ m^{-1} for the cross-shore velocities.

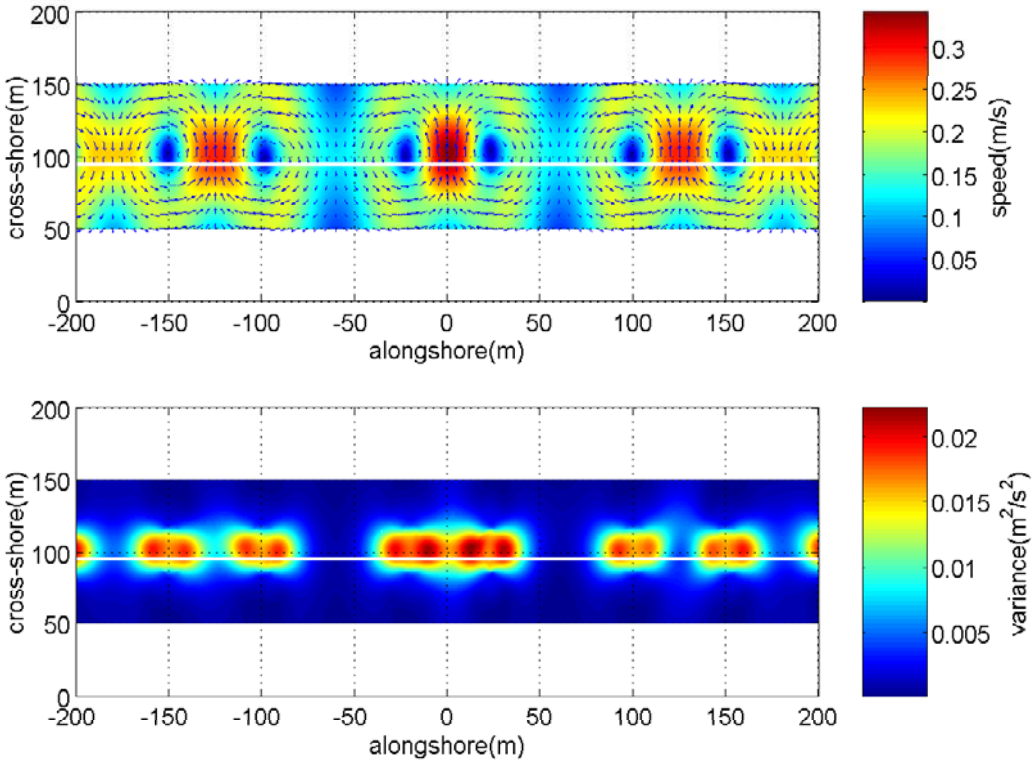

Figure 14. (top) The mean flow structure of the conceptual model of rip current velocity cells based on equations (1)–(3). (bottom) The variance of the velocity field. Solid line is the location for computations of the two-dimensional FFT representative of the location of the alongshore array in the field.

sinusoidal curve which oscillates at a particular frequency (VLF), and it is relatively fixed in space, which is associated with the rip current spacings. The alongshore velocities will remain relatively the same, except there will be a slight alongshore displacement, which smears the energy around $k_y = 0$ m^{-1} (Figures 11–12). This indicates that there is morphological feedback coupled with the rip current eddy cells, as they are topographically controlled by the shore-connected shoals and rip channels, but there is relaxation within the hydrodynamics to allow the rip current cells to move. Thus the SZEs at RIPEX are being forced by radiation stress gradients associated with breaking of wave groups and are not free eddies traveling along the coast.

4.2. Kinematic Conceptual Model

[28] A conceptual model of rip current cell circulations is developed to aid in interpreting the SZE behavior observed in the f-k_y spectral observations (see Figures 11 and 12). In the model a two-dimensional Gaussian stream function is utilized to describe the cells, defined by

$$\Psi(x,y,t) = \sum_{n=1}^{N} -1^n A e^{-\lambda\left([x-x_c(n,t)]^2+[y(t)-y_c(n,t)]^2\right)}, \qquad (1)$$

where N is the number of cells, -1^n makes the field spatially periodic, A is a constant amplitude of the Gaussian field, λ is the length of the cell, x_c, y_c represents the center of the cells, and t is time. Assuming a rigid lid, velocities are defined as stream function derivatives,

$$u = -\frac{\partial \Psi}{\partial y}, v = \frac{\partial \Psi}{\partial x}. \qquad (2)$$

Each rip current cell is converted into velocity vectors. Multiple rip current cells are located in space, representing the approximate locations of rip currents in the RIPEX bathymetry (Figure 2). The overlapping of neighboring rip currents cells is additive, such that the section of cells located in close proximity are faster than cells with sections which are further apart (superposition) (Figure 14 (top)). Rip current cells are separated in the vicinity of onshore transport (shore-connected shoals) and close together for offshore transport (rip channels), producing faster offshore directed flows (representative of rip currents). The model has regions of zero velocity, which would not be the case in nature.

[29] The center (x_c, y_c) of each rip current cell is sinusoidally oscillated in time,

$$x_c(n,t)[y_c(n,t)] = \sum_{k=1}^{12} dX_k[dY_k]\sin(f_k 2\pi t + \varepsilon_k), \qquad (3)$$

with uniform random distributions of amplitudes (dX_k, dY_k), frequencies ($0 \le f_k \le 0.004$ Hz), and phases (ε_k), which cause the rip current cells to oscillate in the cross-shore and alongshore directions. Here dX and dY are the potential maximum amplitudes of the uniform distributions. Simulations were run for approximately two hours with a sampling interval of 5 s, similar to field velocity measurements for the f-k_y spectra. F-k_y spectral estimates are computed using two-dimensional (2-D) fast-Fourier tansforms (FFTs) with a hamming window resulting in 40 DOF with $df = 0.0004$ Hz for measurements along $y = 88$ in Figure 14 (solid line). $F - k_y$ spectra represent the fluctuations associated with the system, not the mean flow structure of the rip current cells

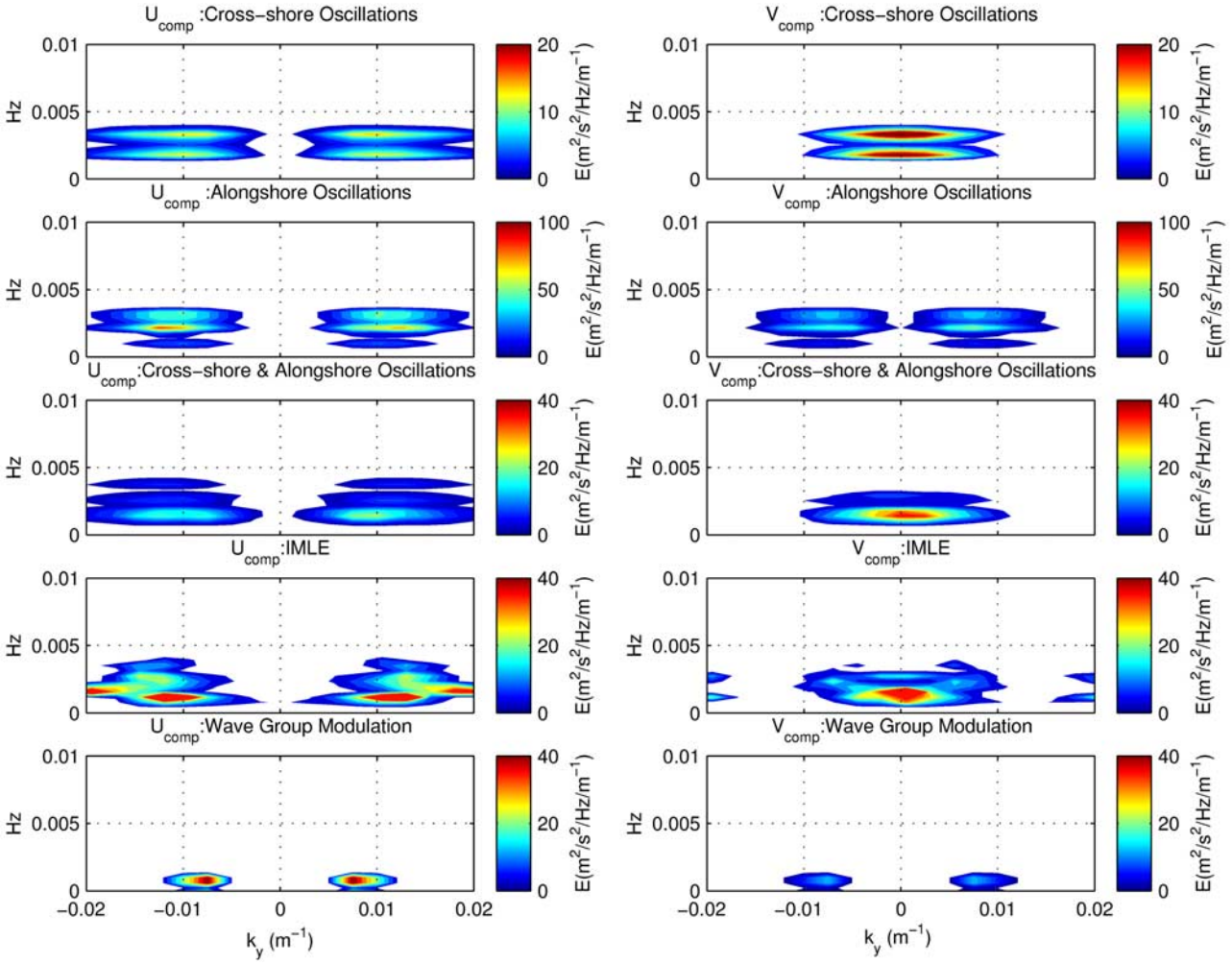

Figure 15. $F - k_y$ spectral estimates using 2-D FFT of kinematic conceptual models of rip current cell oscillations; (first row) oscillations of cross-shore rip current cell dX = 15 m, dY = 0 m, (second row) oscillations of alongshore rip current cell dX = 0 m, dY = 15 m, (third row) cross-shore and alongshore oscillation of rip current cells dX = 15 m, dY = 4 m, (fourth row) IMLE for the cross-shore and alongshore oscillation of rip current cells dX = 15 m, dY = 4 m, (fifth row) 2-D FFT for VLF amplitude, $A(t)$, modulations of rip current cells.

(Figure 14). Three scenarios were numerically performed: (1) rip current cells that only oscillate randomly in the cross-shore (dX = 15 m, dY = 0 m), (2) rip current cells that only oscillate randomly in the alongshore (dX = 0 m, dY = 15 m), and (3) rip currents cells that oscillate randomly in both directions (dX = 15 m, dY = 4 m).

[30] The results indicate that when the rip current cells only oscillate in the cross shore, the k_y of the cross-shore velocities is equivalent to the rip current spacings, while the k_y of the alongshore velocities is spread around zero (Figure 15 (top)). This is similar to the measurements obtained from the alongshore array of the field experiment (Figure 11). For strictly alongshore oscillations (Figure 15 (second panel)), k_y is focused around rip current spacing for both cross-shore and alongshore velocities. A scenario with equal cross-shore and alongshore movements was also performed (not shown), which produced results similar to the case with just alongshore oscillations (Figure 15 (second panel)). The last case is for a slight amount of alongshore oscillation (4 m) dominated by cross-shore oscillation (15 m) and tends to smears the f-k_y spectra (Figure 15 (third panel)), which are most comparable to the field measurements (Figure 11). The IMLE method was performed on the last case with a spatial array similar to the field array (Figure 1) with some additional locations that span the entire alongshore domain (Figure 15 (fourth panel)). The IMLE has similar results to that of the 2-D FFT but with more localized energy within k_y. This suggests a plausible description that during the experiment the rip current cells randomly oscillated in the cross shore with smaller alongshore oscillations.

4.3. SZE Wave Group Behavior

[31] Another potential mechanism that can explain the SZE motions is that slow modulations in wave group energy increase the velocities of the rip current cells through pressure and radiation stress gradients [*Bowen*, 1969]. The randomness of the wave groups produce durations of large

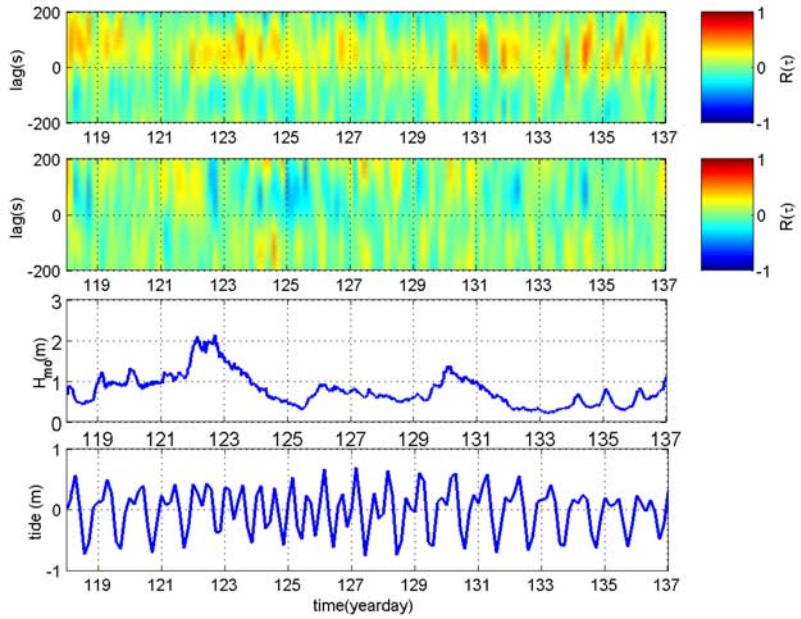

Figure 16. Contours (color scale at the right) of cross-correlation functions for: (first row) VLF offshore wave group energy (PUV4) and rip channel cross-shore VLF velocity (PUV11); (second row) VLF offshore wave group energy (PUV4) and rip channel alongshore VLF velocity (PUV11) as a function of lag and time; (third row) H_{mo} measured at the buoy versus time; and (fourth row) tidal elevation versus time.

energy followed by durations with less energy, which would be expected to induce a slowly varying rip current velocity field. This would appear as though the rip current cells were oscillating in the cross shore as described by the conceptual model. To examine this mechanism, a modulation of Gaussian amplitude (A) is applied to equation (1), keeping the center of the cells fixed, where

$$A(t) = A_o + A' \sin(\omega t + \epsilon), \tag{4}$$

where A_o is a constant, A' is the modulation amplitude, ω is the radian frequency with the VLF band, and ϵ is the phase of the system. The VLF amplitude modulation results in energy focused around the rip channel spacings for both cross-shore and alongshore velocities in f-k_y space (Figure 15 (bottom panel)). Though the energy is larger in the cross-shore velocity, the spatial pattern does not match the field observations.

[32] Cross-correlation functions were computed between the VLF wave group energy, $E(t)$, at PUV4 and U_{VLF} within the rip channel at PUV11, plotted as a time stack (Figure 16). There is a positive correlation occurring at ~50 s, which is theoretical time for wave group energy to propagate from PUV4 to PUV11 [*MacMahan et al.*, 2004]. VLF modulations of wave group energy are correlated for the slow oscillations of the rip current cells. However, there is no clear trends associated with the correlation, in particular during times of increased wave energy, when the SZE energy increases. The temporal variation of wave group energy is only part of the mechanism; the influences of the Δk_y also induce random eddies into the surf zone at VLF frequencies [*Reniers et al.*, 2004]. Thus it is the spatial and temporal aspects of the wave groups and their coupling with the underlying bathymetry, which force the SZE oscillations, as explained by the kinematic conceptual model.

4.4. Jet Instability

[33] In addition to the rip current cell oscillations (described above), jet instabilities may be associated with smaller surf zone eddies. In a laboratory experiment, *Haller and Dalrymple* [2001] found that topographically controlled rip currents [*Haller et al.*, 2002] forced by monochromatic waves were often unstable. They obtained good comparisons of their observations with a model based on the linear instability theory of a narrow jet. *Chen et al.* [1999] obtained good agreement with the same laboratory measurements of rip currents using the fully nonlinear Boussinesq formulation. *Yu and Slinn*'s [2003] numerical evaluation of wave-current interactions of rip current flows indicates that the rip current instabilities originate within the feeder channels and migrate offshore.

[34] Some of the laboratory observations by *Haller and Dalrymple* [2001] resemble the field observations. However, in the laboratory, the instabilities are concentrated within the rip channel neck and decrease in intensity over the neighboring bars, while in the field the SZEs are of similar magnitude, regardless of sensor location within the surf zone (Figure 8). This may be a result of the relative close proximity of rip current cells in the field ($\lambda_r/w_r = 2$) (Figure 2), which were not completely independent, whereas the rip current systems in the laboratory were relatively independent ($\lambda_r/w_r = 5$), where λ_r is the rip channel spacing and w_r is the rip channel width. The characteristics of the morphology are also different. The laboratory experiment morphology is a longshore-trough bar with straight rip channels cutting through the bar, which may confine the flow more than the complex morphology of a shore-connected

shoal with smaller feeder channels and incised rip channels that increase in width as a function of cross-shore distance.

[35] The *Haller et al.* [2002] laboratory measurements are scaled using an undistorted Froude number (Fr = 0.2–0.6) with a length scale ratio of 1/50, which corresponds to a rip current system in nature having 450 m rip spacing, 90 m rip width, breaking wave heights 1.3–3.8 m, wave periods of 5.7–7.1 s, and mean rip current velocities of 1.0–2.1 m/s. This is different than the field conditions during the RIPEX field experiment. During RIPEX the rip channel system corresponded to a rip current spacing of 125 m, 60 m rip current width, wave heights at P5 of 0.3–2 m, 4–10 s wave period, 0–1 m/s mean rip current velocities, resulting in Fr = 0–0.45.

[36] The largest difference between the field and laboratory scaled rip currents is the flow speeds, which may be a result of the differences in geometry, rip channel alongshore spacing, width of channel, width of bar, and depth of channel. This results in significant differences in rip current shear, computed as the mean velocity within the rip channel divided by the width of the rip channel. The shear for the laboratory was 0.11 m/s/m for a 0.2 m/s rip flow and a 1.82 m rip channel width, while in the field during RIPEX the shear was 0.008 m/s/m for a 0.5 m/s rip flow and a 60 m rip channel width. This order of magnitude difference suggests that the mechanisms responsible for the instabilities may be different as well as their spatial occurrences. Furthermore, the wave forcing is also different, as the laboratory experiment used monochromatic waves and field conditions consisted of directionally broad wave groups. Thus the field observations of VLF SZEs do not appear to be associated with jet instabilities.

5. Summary and Conclusion

[37] Energetic motions at the very low frequency (<0.004 Hz) were observed throughout the RIPEX experiment. SZEs were present everywhere on the beach system, composed of shore-connected shoals with incised rip channels. SZE velocities were ~25 cm/s within the surf zone with alongshore homogeneity and decreases to ~5 cm/s outside of the surf zone. The SZE cross-shore velocity energy is concentrated within the very low frequency band (<0.004 Hz) and with alongshore wave number corresponding to the morphodynamic scale of rip channels, differing from observations of the energy of shear instabilities of the longshore current residing at higher frequencies [*Oltman-Shay et al.*, 1989]. Insignificant mean longshore currents were present during the field measurements to generate longshore current instabilities. Previous field measurements of rip currents seem to have documented SZEs, but a conclusive interpretation was not available [*Smith and Largier*, 1995; *Brander and Short*, 2001]. *Haller and Dalrymple* [2001] illustrated through detailed measurements in a laboratory and an analytical model that the jet-like flow of the rip current can be unstable. These field measurements of SZEs differ from the laboratory measurements by morphological and hydrodynamic scales, λ_r/w_r, Fr, and a order of magnitude difference in shear.

[38] SZE energy increases with increasing sea-swell energy and with some possible tidal modulation. There is a weaker statistically significant correlation between SZE velocity variation and U_{mean} (Figure 9). A better correlation exists between $U_{\mathrm{rms,VLF}}$ and H_o (Figure 9), indicating that wave forcing may be responsible for triggering the rip current cell oscillation. The alongshore velocities are correlated in the alongshore when the SZEs are most energetic (Figure 10), while the cross-shore velocities are out-of-phase between the rip channels and the shore-connected shoals (Figure 10). F-k_y spectra indicate that the SZEs of the cross-shore velocities are coupled to the spacing of the rip current channels (k_y = ±0.008 m^{-1}), while alongshore velocities are concentrated around k_y = 0 m^{-1} (Figures 11–12). A simple kinematic conceptual model (Figure 13) of the entire rip current system oscillating produced results similar to the field observations (Figure 14). The best comparison were formed when the rip current cells tend to oscillate more in the cross shore than in the alongshore (Figures 11, 12, and 15).

[39] **Acknowledgments.** We extend our appreciation to the many folks who assisted in obtaining a great data set: Loraine Chial, Ron Cowen, Jason Engle, James Joyner, Gregory Miller, Tom Lippmann, Denis Morichon, Bruce Morris, Mark Orzech, Jennifer Short, Sidney Schofield, Jim Stockel, Charlotte Webb, Rob Wyland, and volunteers for Hopkins Marine Station (Stanford University) led by Mark Denny. We thank Tom Herbers and Paul Jessen for providing offshore buoy data. And a special thanks to Edie Gallagher for leading the survey work. The Steep Beach Experiment was funded by the Office of Naval Research (ONR), Coastal Sciences Program under contract N0001402WR20188 and data analysis the National Science Foundation under contract OCE-01366882 and ONR. JM was funded by the National Science Foundation under contract OCE-01366882. AR held a National Research Council-NPS Research Associateship funded by ONR and National Ocean Partnership Program (NOPP-N0001404WR20125). Additional funding for AR was provided by the Dutch Organization of Scientific Research (NWO) under contract DCB.5856. We thank Jim Kirby and the two anonymous reviewers for their useful comments and suggestions.

References

Aagaard, T., B. Greenwood, and J. Nielsen (1997), Mean currents and sediment transport in a rip channel, *Mar. Geol.*, *140*, 24–45.

Beach, R. A., and R. W. Sternberg (1988), Suspended sediment transport in the surf zone: Response to cross-shore infragravity motion, *Mar. Geol.*, *80*, 61–79.

Bowen, A. J. (1969), Rip currents: 1. Theoretical investigations, *J. Geophys. Res.*, *74*, 5467–5478.

Bowen, A. J., and R. A. Holman (1989), Shear instabilities of the mean longshore current: Theory, *J. Geophys. Res.*, *94*, 18,023–18,030.

Brander, R. W. (1999), Field observations on the morphodynamic evolution of low wave energy rip current system, *Mar. Geol.*, *157*, 199–217.

Brander, R. W., and A. D. Short (2000), Morphodynamics of a large-scale rip current system at Muriwai Beach, New Zealand, *Mar. Geol.*, *165*, 27–39.

Brander, R. W., and A. D. Short (2001), Flow kinematics of low-energy rip current systems, *J. Coastal Res.*, *17*(2), 468–481.

Buhler, O., and T. E. Jacobson (2001), Wave-driven currents and vortex dynamics on barred beaches, *J. Fluid Mech.*, *449*, 313–339.

Chen, Q., R. A. Dalrymple, J. T. Kirby, A. B. Kennedy, and M. C. Haller (1999), Boussinesq modeling of a rip current system, *J. Geophys. Res.*, *104*, 20,617–20,637.

Dalrymple, R. A. (1975), A mechanism for rip current generation on an open coast, *J. Geophys. Res.*, *80*, 3485–3487.

Dronen, N., H. Karunarathna, J. Fredsoe, B. M. Sumer, and R. Deigaard (2002), An experimental study of rip channel flow, *Coastal Eng.*, *45*(3–4), 223–238.

Fowler, R. E. (1991), Wave group forced nearshore circulation: A generation mechanism for migrating rip currents and low frequency motion, *Fin. Rep., Res. Rep. #CACR–91–03*, Cent. for Appl. Coastal Res., Univ. of Del., Newark.

Fowler, R. E., and R. A. Dalrymple (1990), Wave group forced nearshore circulation, in *Proceedings of the 22nd International Conference on Coastal Engineering*, pp. 729–742, Am. Soc. of Civ. Eng., Reston, Va.

Guza, R. T., and E. B. Thornton (1985), Observations of surf beat, *J. Geophys. Res.*, *90*, 3161–3171.

Haller, M. C., and R. A. Dalrymple (2001), Rip current instabilities, *J. Fluid Mech.*, *433*, 161–192.

Haller, M. C., R. A. Dalrymple, and I. A. Svendsen (2002), Experimental study of nearshore dynamics on a barred beach with rip channels, *J. Geophys. Res.*, *107*(C6), 3061, doi:10.1029/2001JC000955.

Holman, R. A. (1981), Infragravity energy in the surfzone, *J. Geophys. Res.*, *86*, 6442–6450.

Huntley, D. A. (1976), Long-period waves on a natural beach, *J. Geophys. Res.*, *81*, 6441–6449.

Huntley, D. A., R. T. Guza, and E. B. Thornton (1981), Field observations of surf beat: 1. Progressive edge waves, *J. Geophys. Res.*, *86*, 6451–6466.

MacMahan, J. (2001), Hydrographic surveying from a personal watercraft, *J. Surv. Eng.*, *127*(1), 12–24.

MacMahan, J. H., A. J. H. M. Reniers, E. B. Thornton, and T. P. Stanton (2004), Infragravity rip current pulsations, *J. Geophys. Res.*, *109*, C01033, doi:10.1029/2003JC002068.

Noyes, T. J., R. T. Guza, S. Elgar, and T. H. C. Herbers (2004), Field observations of shear waves in the surf zone, *J. Geophys. Res.*, *109*, C01031, doi:10.1029/2002JC001761.

Ogston, A. S., and R. W. Sternberg (2003), Nearshore sediment suspension and flux in response to low-infragravity frequency and episodic processes: Exploratory analysis, in *Coastal Sediment* [CD-ROM], Am. Soc. of Civ. Eng., Reston, Va.

Oltman-Shay, J., and R. T. Guza (1987), Infragravity edge wave observations on two California beaches, *J. Phys. Oceanogr.*, *17*, 644–663.

Oltman-Shay, J., P. A. Howd, and W. A. Birkemeier (1989), Shear instabilities of mean longshore current: 2. Field observations, *J. Geophys. Res.*, *94*, 18,031–18,042.

Pakwa, S. S. (1983), Island shadows in wave directional spectra, *J. Geophys. Res.*, *88*, 2579–2591.

Peregrine, D. H. (1998), Surf zone currents, *Theor. Comput. Fluid Dyn.*, *10*, 295–309.

Reniers, A. J. H. M., J. A. Roelvink, and E. B. Thornton (2004), Morphodynamic modeling of an embayed beach under wave group forcing, *J. Geophys. Res.*, *109*, C01030, doi:10.1029/2002JC001586.

Ryrie, S. C. (1983), Longshore motion due to an obliquely incident wave group, *J. Fluid Mech.*, *137*, 273–284.

Shepard, F. P., and D. L. Inman (1950), Nearshore water circulation related to bottom topography and refraction, *Eos Trans. AGU*, *31*, 196–212.

Smith, J. A., and J. L. Largier (1995), Observations of nearshore circulation: Rip currents, *J. Geophys. Res.*, *100*, 10,967–10,975.

Sonu, C. J. (1972), Field observations of nearshore circulation and meandering currents, *J. Geophys. Res.*, *77*, 3232–3247.

Suhayda, J. N. (1974), Standing waves on beaches, *J. Geophys. Res.*, *79*, 3065–3071.

Tang, E. C.-S., and R. A. Dalrymple (1989), Nearshore circulation: Rip currents and wave groups, in *Nearshore Sediment Transport*, edited by R. J. Seymour, pp. 205–229, Plenum, New York.

Wright, L. D., R. T. Guza, and A. D. Short (1982), Dynamics of high-energy dissipative surf zone, *Mar. Geol.*, *45*, 41–62.

Yu, J., and D. N. Slinn (2003), Effects of wave-current interaction on rip currents, *J. Geophys. Res.*, *108*(C3), 3088, doi:10.1029/2001JC001105.

J. H. MacMahan, T. P. Stanton, and E. B. Thornton, Oceanography Department, Naval Postgraduate School, Monterey, CA 93943, USA. (jhmacmah@nps.edu)

A. J. H. M. Reniers, Civil Engineering and Geosciences, Delft University of Technology, Delft ZH 2628CN, Netherlands.